Environmental Pollution 244 (2019) 783–791

Contents lists available at ScienceDirect

Environmental Pollution

journal homepage: www.elsevier.com/locate/envpol

Cd^{2+} adsorption performance of tunnel-structured manganese oxides driven by electrochemically controlled redox☆

Lihu Liu [a], Qichuan Peng [a], Guohong Qiu [a, *], Jun Zhu [a], Wenfeng Tan [a], Chengshuai Liu [b], Lirong Zheng [c], Zhi Dang [d]

[a] Key Laboratory of Arable Land Conservation (Middle and Lower Reaches of Yangtse River), Ministry of Agriculture, Hubei Key Laboratory of Soil Environment and Pollution Remediation, College of Resources and Environment, Huazhong Agricultural University, Wuhan, 430070, Hubei Province, China
[b] State Key Laboratory of Environmental Geochemistry, Institute of Geochemistry, Chinese Academy of Sciences, Guiyang, 550081, China
[c] Beijing Synchrotron Radiation Facility, Institute of High Energy Physics, Chinese Academy of Sciences, Beijing, 100039, China
[d] School of Environment and Energy, South China University of Technology, Guangzhou, 510006, China

ARTICLE INFO

Article history:
Received 2 August 2018
Received in revised form
27 September 2018
Accepted 12 October 2018
Available online 24 October 2018

Keywords:
Heavy metal ions
Electrochemical adsorption
Cryptomelane
Todorokite
Pyrolusite

ABSTRACT

The heavy metal ion adsorption performance of birnessite (a layer-structured manganese oxide) can be enhanced by decreasing the Mn average oxidation state (Mn AOS) and dissolution–recrystallization during electrochemical redox reactions. However, the electrochemical adsorption processes of heavy metal ions by tunnel-structured manganese oxides are still enigmatic. Here, tunnel-structured manganese oxides including pyrolusite (2.3 Å × 2.3 Å tunnel), cryptomelane (4.6 Å × 4.6 Å tunnel) and todorokite (6.9 Å × 6.9 Å tunnel) were synthesized, and their electrochemical adsorptions for Cd^{2+} were performed through galvanostatic charge–discharge. The influence of both supporting ion species in the tunnel and tunnel size on the electrochemical adsorption performance was also studied. The adsorption capacity of tunnel-structured manganese oxides for Cd^{2+} was remarkably enhanced by electrochemical redox reactions. Relative to K^+ in the tunnel of cryptomelane, the supporting ion H^+ was more favorable to the electrochemical adsorption of Cd^{2+}. With increasing initial pH and specific surface area, the electrochemical adsorption capacity of cryptomelane increased. The cryptomelane electrode could be regenerated by galvanostatic charge–discharge in Na_2SO_4 solution. Due to the differences in their tunnel size and supporting ion species, the tunnel-structured manganese oxides follow the order of cryptomelane (192.0 mg g^{-1}) > todorokite (44.8 mg g^{-1}) > pyrolusite (13.5 mg g^{-1}) in their electrochemical adsorption capacities for Cd^{2+}.

1. Introduction

Contamination of water by heavy metal ions is posing serious threats to human health (Guo et al., 2016; Ihsanullah et al., 2016; Wang et al., 2016). Heavy metal ions can be accumulated in ecosystems and living organisms due to their non-biodegradable properties (Wang et al., 2016; Ye et al., 2017). Cd^{2+} is a highly toxic heavy metal ion without any known nutritional function, and its half-life in human body is estimated to be 4–38 years (Riederer et al., 2013). The main source of Cd^{2+} in drinking water is wastewater discharged from industries (Ihsanullah et al., 2016; Riederer et al., 2013; Wang et al., 2016). A concentration of 0.005 mg L^{-1} was recommended as the limitation of Cd^{2+} in drinking water by WHO (World Health Organization) (Mohan and Singh, 2002). Cd^{2+} accumulation may cause renal abnormality and itai-itai disease in human (Ihsanullah et al., 2016; Riederer et al., 2013). Hence, excessive Cd^{2+} should be recovered or removed as much as possible from wastewaters before being discharged into the environment.

Adsorption is regarded as an appropriate option for treating wastewaters contaminated by heavy metal ions due to its advantages of easy operation and low cost (Ihsanullah et al., 2016; Wan et al., 2016; Wang et al., 2016). Electrochemical adsorption, which combines electrochemical techniques and adsorption, is a promising water treatment technology. Characterized by less energy consumption, high efficiency and no secondary pollution, electrochemical adsorption has been widely applied to remove organics (López-Bernabeu et al., 2016), salt ions (Zhang et al., 2018), and

☆ This paper has been recommended for acceptance by Joerg Rinklebe.
* Corresponding author.
E-mail address: qiugh@mail.hzau.edu.cn (G. Qiu).

https://doi.org/10.1016/j.envpol.2018.10.062
0269-7491/

heavy metal ions (Gaikwad and Balomajumder, 2017; Hu et al., 2015).

Manganese oxides are extensively studied for cation adsorption owing to their low point of zero charge, abundant availability and eco-friendliness (Kim et al., 2013; Wan et al., 2016; Wang et al., 2013; Zhao et al., 2012). The application of electric field can improve their adsorption performance (Hu et al., 2015; Liu et al., 2017a; Liu et al., 2017b; Peng et al., 2016). For example, the Cu^{2+} adsorption capacity of MnO_2/carbon fiber could be enhanced to 172.9 mg g^{-1} by applying the voltage of −0.8 V (Hu et al., 2015). MnO_2/carbon nanotube composite showed a high electrochemical adsorption capacity (6.65 mg g^{-1}) for NaCl (Chen et al., 2016). The excellent electrochemical adsorption performance of manganese oxides can be attributed to the suitable pore structure and large specific surface area by previous studies (Chen et al., 2016; Hu et al., 2015).

Recently, redox reactions were found to contribute much to the electrochemical adsorption of manganese oxides for salt ions (Zhang et al., 2018). Our previous studies have indicated that the decrease in Mn AOS and dissolution–recrystallization could facilitate the heavy metal ion adsorption of layer-structured birnessite during electrochemical redox reactions (Liu et al., 2017a; Liu et al., 2017b; Yang et al., 2018). The adsorption capacities of birnessite/carbon nanotube composite for Ni^{2+} and Zn^{2+} could respectively reach 158.4 and 155.6 mg g^{-1} by constant-potential electrolysis (Liu et al., 2017b). The adsorption capacities of birnessite for Cu^{2+}, Cd^{2+} and Zn^{2+} could be respectively elevated to 372.3, 900.7 and 530.0 mg g^{-1} by galvanostatic charge–discharge, which are about 8–10 times higher than their adsorption isotherm capacities (Liu et al., 2017a; Peng et al., 2016; Yang et al., 2018). Therefore, the heavy metal ion adsorption of manganese oxides can be influenced by electrochemical redox reactions.

There are layer- and tunnel-structured manganese (IV) oxides according to the stacking mode of MnO_6 octahedra (Post, 1999). Birnessite, buserite and vernadite are common layer-structured manganese oxides (Post, 1999), and pyrolusite, cryptomelane and todorokite are common tunnel-structured manganese oxides (Ghodbane et al., 2009). Their electrochemical redox properties are different due to the differences in their crystal structure (Ghodbane et al., 2009; Qiu et al., 2011). Generally, when manganese (IV) oxides are used as electrode materials for pseudocapacitors, the specific capacitance follows the order of birnessite > ramsdellite > cryptomelane > todorokite > pyrolusite (Ghodbane et al., 2009). Hence, the electrochemical adsorption processes of tunnel- and layer-structured manganese oxides may be different.

There are differences in chemical composition and tunnel size between pyrolusite (2.3 Å × 2.3 Å tunnel), cryptomelane (4.6 Å × 4.6 Å tunnel) and todorokite (6.9 Å × 6.9 Å tunnel). Therefore, they were used for the electrochemical adsorption of Cd^{2+} by galvanostatic charge–discharge. This study aims to clarify the influencing factors and mechanisms of the electrochemical adsorption for heavy metal ions by tunnel-structured manganese oxides. The micromorphology, crystal structure and chemical composition after electrochemical adsorption were characterized by field emission scanning electron microscopy (FESEM), X-ray diffractometer (XRD) and X-ray absorption spectroscopy (XAS).

2. Experimental

2.1. Preparation of manganese oxides

Cryptomelane was synthesized through a modified microwave-hydrothermal reaction (Dharmarathna et al., 2012). The mixed solution containing 0.1/0.5/1.0 mol L^{-1} H_2SO_4, 0.02 mol L^{-1} $MnSO_4$ and 0.02 mol L^{-1} $KMnO_4$ with a volume of 50 mL was added into an 80-mL vessel. Then, the vessel was transferred into a CEM Discover microwave reactor. The reaction temperature and time were set as 120 °C and 20 min, respectively. The resulting solid was collected and washed with distilled deionized water, and then dried at 60 °C. The obtained cryptomelane was respectively designated as 0.1Cry, 0.5Cry and 1.0Cry when the H_2SO_4 concentration in the reaction system was 0.1, 0.5 and 1.0 mol L^{-1}, respectively. Pyrolusite and todorokite were respectively synthesized by hydrothermal reaction of $MnSO_4$ and $(NH_4)_2S_2O_8$ and refluxing process from Mg-buserite according to the procedures previoulsy reported (Feng et al., 2004; Wang and Li, 2002).

2.2. Electrochemically controlled adsorption of Cd^{2+}

A three-electrode system (30 mL in volume) was used to perform the electrochemical adsorption of Cd^{2+} at room temperature. The synthesized manganese oxides (75 wt.%), acetylene black (15 wt.%) and polyvinylidene fluoride (10 wt.%) were dispersed into 1-methyl-2-pyrrolidinone. The prepared mixture was coated on carbon fabric (1.5 × 2.5 cm^2) to prepare the working electrode. The mass of manganese oxide on each electrode was controlled to be 5 mg. Saturated calomel electrode (SCE) and blank carbon fabric (1.5 × 2.5 cm^2) were respectively used as the reference and counter electrodes.

Cd-containing solutions were prepared by dissolving the $CdSO_4$ into 0.1 mol L^{-1} Na_2SO_4 solution. The initial concentration of Cd^{2+} varied from 0 to 1000 mg L^{-1}. 0.1 mol L^{-1} H_2SO_4/NaOH solution was used to adjust the initial pH of the above solutions to 5.0. In order to investigate the effect of pH on the electrochemical adsorption capacity of cryptomelane, the initial pH was controlled to be 2.0, 3.0, 4.0, 5.0 and 6.0. The electrochemical adsorption was conducted by galvanostatic charge–discharge on a CT-3008W-5V5mA battery testing system (Shenzhen Neware Electronic Ltd., China). The current density and potential window were 0–0.9 V (*vs.* SCE) and 0.1 A g^{-1}, respectively. After electrochemical adsorption, the working electrode was washed and characterized by XRD. The samples were kept in a vacuum bag after drying in a vacuum oven.

The regeneration performance of cryptomelane electrode was evaluated by the cycle operation of electrochemical adsorption–desorption. The electrochemical adsorption and desorption were performed in 1000 mg L^{-1} Cd^{2+} solution and 0.1 mol L^{-1} Na_2SO_4 solution, respectively. The electrochemical adsorption of 1.0Cry with the ion exchange of H^+ by K^+ was performed at initial pH 5.0 to investigate the effect of supporting ion K^+ in the tunnel on the adsorption performance of cryptomelane. To exchange the H^+ in the tunnel with K^+, 1.0Cry (0.034 g) was placed into K_2SO_4 solution (0.5 mol L^{-1}, 50 mL) and stirred for 24 h.

The isothermal adsorption of Cd^{2+} on cryptomelane was conducted at constant pH 5.0, and the adsorption process and capacity were compared with those of electrochemical adsorption. The detailed process of isothermal adsorption and calculation of Cd^{2+} adsorption capacity (Equation S(1)) were presented in the Supporting Information.

2.3. Characterization

The Mn AOS in the manganese oxides was determined by chemical titration using a $KMnO_4$ standard solution (Kijima et al., 2001). The concentrations of Mn^{2+} and Cd^{2+} in the solutions were determined by Varian AAS240FS atomic absorption spectroscopy. The pristine cryptomelane and cryptomelane electrodes after electrochemical adsorption were digested in a microwave oven (Mars6, CEM) at 190 °C, and the K^+ concentration was determined by Sherwood 410 Flame photometer.

The crystal structures, functional groups and specific surface

areas of samples were analyzed using D8 ADVANCE diffractor (Bruker, Cu Kα), VERTEX 70 Fourier transform infrared spectroscopy (FTIR, Bruker) and Micromeritics ASAP 2020, respectively. The changes in micromorphology of the manganese oxides during electrochemical adsorption were analyzed by SU8000 FESEM (HITACHI) and Talos F200C transmission electron microscopy (TEM, FEI). XAS measurement was conducted under air atmosphere on 1W1B beamline at the Beijing Synchrotron Radiation Facility, China. The detailed collection and analyses of XAS were shown in Supporting Information.

3. Results

3.1. Manganese oxide characterization

The XRD and FTIR results indicated that single-phase cryptomelane (JCPDS card No. 74–1451), todorokite (JCPDS card No. 38–0475) and pyrolusite (JCPDS card No. 81–2261) were obtained (Fig. 1 and Fig. S1). Rietveld structure refinement of 0.1Cry, 0.5Cry and 1.0Cry was conducted using software TOPAS from Bruker. The monoclinic symmetry (*I* 2/m) structure was used in the Rietveld structure refinement process (Fig. 1a). As presented in Table 1, with increasing H_2SO_4 concentration in the reaction system, lattice parameters *a* and *β* increased, and no obvious change was observed for lattice parameters *b* and *c*. The cell volume and crystallite size of 0.1Cry and 0.5Cry were not obviously different, but were respectively smaller and larger than those of 1.0Cry.

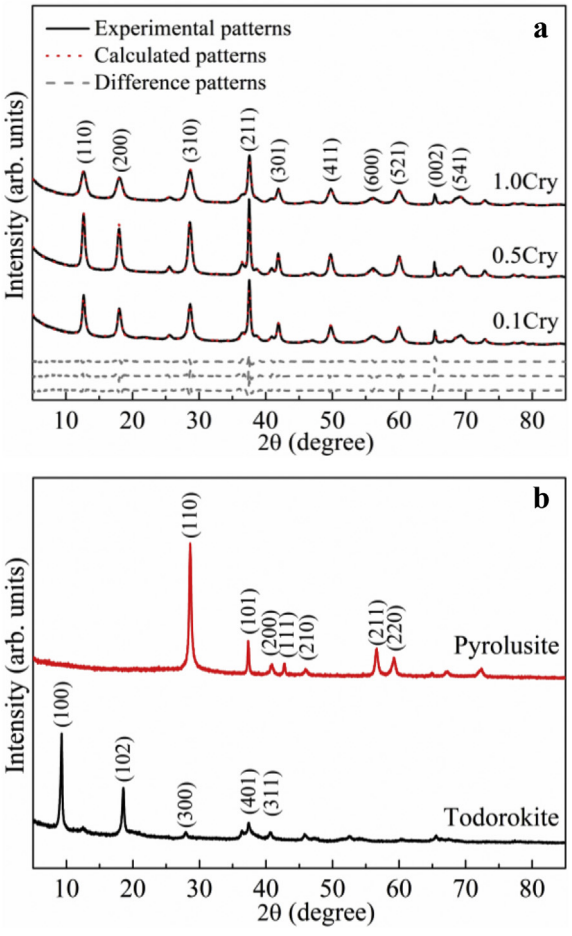

Fig. 1. Rietveld structural refinement of the synthesized cryptomelane (a) and XRD patterns of the synthesized pyrolusite and todorokite (b).

Analysis of chemical composition indicated that the K/Mn molar ratio was 0.08, 0.10 and 0.13 in 0.1Cry, 0.5Cry and 1.0Cry, respectively. According to previous studies, the H^+ in the tunnel of cryptomelane could be exchanged by K^+, and the lattice parameter *a* increases with increasing K^+ content in the tunnel (Poyraz et al., 2017; Yuan et al., 2016), which was also observed in this work (Table 1). The Mg content in todorokite was 4.5 wt.%. The Mn AOS determined by chemical titration method was 3.81 ± 0.04, 3.80 ± 0.03, 3.86 ± 0.01, 3.66 ± 0.02 and 4.04 ± 0.06 for 0.1Cry, 0.5Cry, 1.0Cry, todorokite and pyrolusite, and their specific surface area was 34.1, 38.2, 77.0, 32.2 and 15.1 $m^2\ g^{-1}$, respectively. Fig. S2 shows the FESEM and TEM images of these manganese oxides. Cryptomelane nanowires were obtained (Zhang et al., 2011a; Zhang et al., 2011b), and their lengths showed a downward trend with increasing H_2SO_4 concentration in the synthesis process. Todorokite and pyrolusite showed a nanoflake and a nanorod micromorphology, respectively.

The K/Mn molar ratio of the synthesized cryptomelane increased with increasing H_2SO_4 concentration in the reaction system, which was consistent with our previous work (Qiu et al., 2011). Higher concentration of H_2SO_4 could promote the redox reaction between $MnSO_4$ and $KMnO_4$, resulting in a larger specific surface area of the synthesized cryptomelane, which is likely beneficial to the exchange of H^+ by K^+ in the tunnel.

3.2. Electrochemical adsorption of Cd^{2+} by cryptomelane

The cyclic voltammetry plots of 1.0Cry in Cd^{2+} solutions were shown in Fig. 2a. The cyclic voltammetry plot obtained from the solution without Cd^{2+} showed a relatively rectangular shape, indicating a good redox reversibility of 1.0Cry in Na_2SO_4 solution. With increasing Cd^{2+} concentration, decreases in redox current peaks and redox reversibility were observed in the cyclic voltammetry plots, indicating that the addition of Cd^{2+} could cause decreases in the reversibility of electrochemical redox reactions. The peaks of a_1 and b_1 were respectively assigned to the reduction and oxidation of Mn(IV) and Mn(III,II) (Liu et al., 2017a). During the isothermal adsorption, Cd^{2+} can be adsorbed on the external surface or migrate into the tunnel of cryptomelane (Randall et al., 1998). Therefore, the reduction current peaks a_2 and a_2' might be attributed to Cd^{2+} adsorption on the surface and insertion into the tunnel of cryptomelane. The oxidation current peak b_2 was ascribed the extraction of Cd^{2+} from the surface or tunnel of cryptomelane. Fig. 2b shows the cyclic voltammetry plots of cryptomelane obtained at different H_2SO_4 concentrations. The intensity of redox current peak and the integrated area of cyclic voltammetry increased with increasing H_2SO_4 concentration in the synthesis process. These results indicated that Cd^{2+} can be adsorbed on cryptomelane by electrochemical redox reaction and the redox reactivity in Cd^{2+} solution follows the order of 1.0Cry > 0.5Cry > 0.1Cry (Liu et al., 2016).

Fig. 3a shows the Cd^{2+} adsorption capacities of 0.1Cry, 0.5Cry and 1.0Cry after charge–discharge in Cd^{2+} solutions. The electrochemical adsorption capacity of 1.0Cry was higher than that of 0.1Cry and 0.5Cry. With increasing Cd^{2+} concentration, the electrochemical adsorption capacity of cryptomelane first rose and then reached a plateau. The highest adsorption capacity of 0.1Cry, 0.5Cry and 1.0Cry was 92.3, 95.8 and 192.5 mg g^{-1}, respectively. The final pH of the solution was respectively 4.63, 4.31 and 4.08 after charge–discharge of 0.1Cry, 0.5Cry and 1.0Cry in 1000 mg L^{-1} Cd^{2+} solution. The adsorption isotherm capacity of 0.1Cry, 0.5Cry and 1.0Cry for Cd^{2+} fitted by Langmuir isotherm model was 4.9, 7.6 and 12.2 mg g^{-1}, respectively (Fig. 3b).

Fig. 4a shows the Cd^{2+} adsorption capacity of 1.0Cry after charge–discharge for different cycles in 1000 mg L^{-1} Cd^{2+} solution.

Table 1
Lattice parameters from Rietveld refinement of cryptomelane (*I* 2/m space group).

Sample	*a* (Å)	*b* (Å)	*c* (Å)	*β* (°)	Crystallite size[a] (nm)	Cell volume (Å^3)	R_{wp}[b] (%)
0.1Cry	9.8542(17)	2.8529(32)	9.6833(25)	90.947(16)	22.07(35)	272.19(90)	5.72
0.5Cry	9.8686(13)	2.8550(26)	9.6843(21)	91.005(13)	25.24(30)	272.82(72)	6.65
1.0Cry	9.9290(32)	2.8562(76)	9.6871(39)	91.425(17)	14.96(24)	274.63(16)	5.32

[a] Average coherent scattering domain (CSD) sizes modeled using Lorentzian function.

[b] R_{wp} indicates the quality of fitting and is expressed by $R_{wp} = \sqrt{\frac{\sum w_i(Y_{o,i} - Y_{c,i})^2}{\sum w_i Y_{o,i}^2}}$.

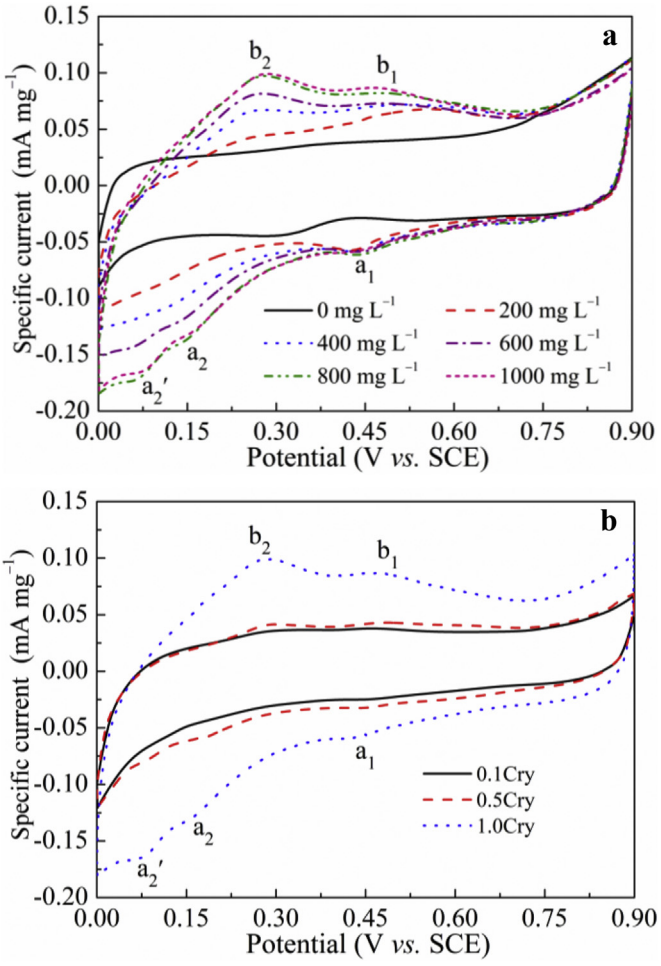

Fig. 2. Cyclic voltammetry plots for the first cycle at a scan rate of 0.5 mV s^{-1} of 1.0Cry in Cd^{2+} solutions with different concentrations (a), and 0.1Cry, 0.5Cry and 1.0Cry in 1000 mg L^{-1} Cd^{2+} solution (b).

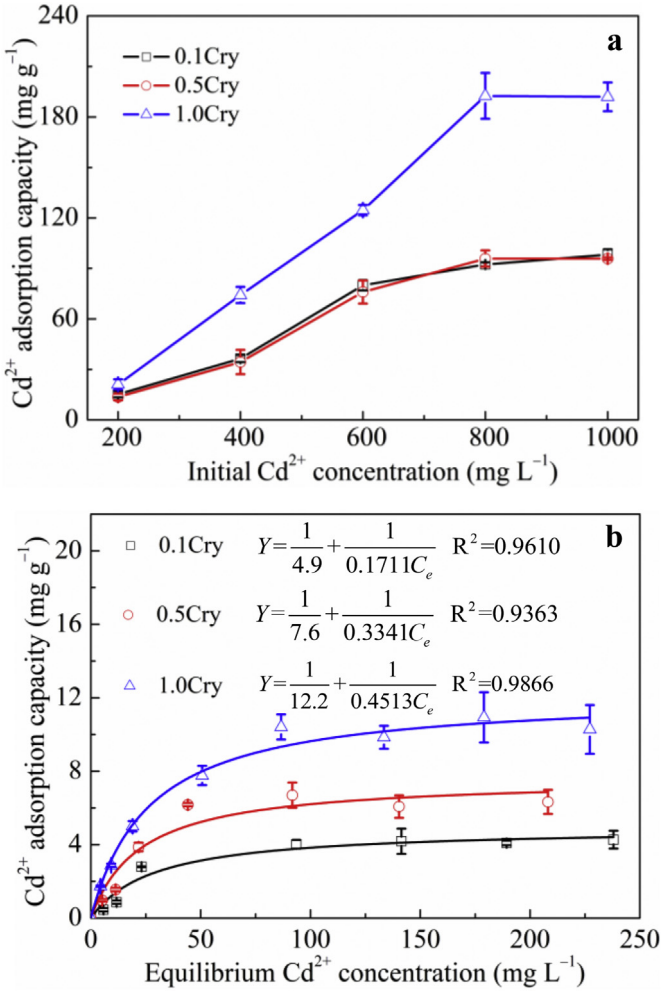

Fig. 3. Cd^{2+} adsorption capacities of cryptomelane after charge–discharge for 50 cycles in Cd^{2+} solutions with different concentrations (a) and isotherms of Cd^{2+} adsorption on cryptomelane (b).

With increasing charge–discharge cycle, the Cd^{2+} adsorption capacity increased and then reached the maximum. These results indicated that the Cd^{2+} adsorption performance of cryptomelane can be remarkably improved by electrochemically controlled redox reactions. Fig. 4b shows the regeneration performance of 1.0Cry electrode. At the fifth cycle of electrochemical adsorption–desorption, the Cd^{2+} adsorption capacity was 38.5 mg g^{-1}, which was higher than the adsorption isotherm capacity (12.2 mg g^{-1}). These results indicated that the cryptomelane electrode can be regenerated.

The content of Mn^{2+} released during Cd^{2+} adsorption was shown in Fig. S3. The highest content of Mn^{2+} released from 0.1Cry, 0.5Cry and 1.0Cry was 18.7, 19.7 and 43.1 mg g^{-1} during the electrochemical adsorption, and was 11.0, 10.7 and 20.6 mg g^{-1} during the isothermal adsorption, respectively. With increases in charge–discharge cycles, the content of released Mn^{2+} increased and then reached a plateau after 20 cycles (Fig. S4). Although the highest content of Mn^{2+} released during the electrochemical adsorption process was about 2 times that during the isothermal adsorption process, the highest Cd^{2+} adsorption capacity during the electrochemical process was nearly 16 times that during the isothermal adsorption process.

The changes in crystal structure, micromorphology and chemical composition of 1.0Cry after electrochemical adsorption were then characterized. Fig. S5 shows the XRD patterns of cryptomelane electrode after electrochemical adsorption. No new diffraction peak was observed, indicating that no transformation product was generated from cryptomelane after electrochemical redox reactions. Fig. 5a–d shows the corresponding FESEM images of 1.0Cry

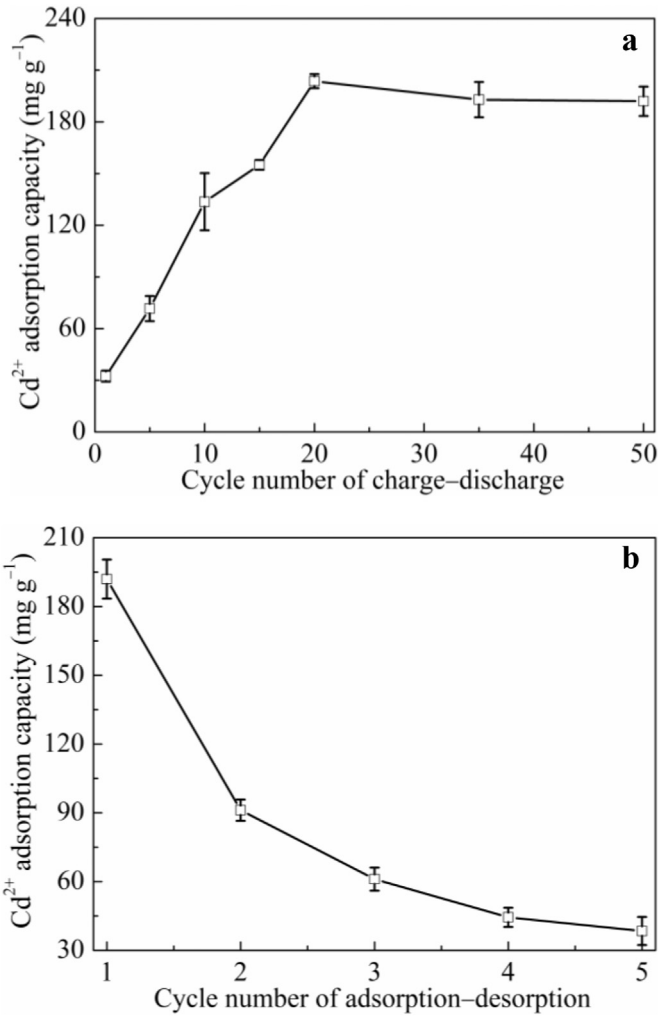

Fig. 4. Cd^{2+} adsorption capacities of 1.0Cry after charge–discharge for different cycles in 1000 mg L^{-1} Cd^{2+} solution (a) and regeneration performance of 1.0Cry electrode (b).

after electrochemical adsorption. The dissolution and transformation of nanowires were observed with increasing Cd^{2+} concentration. There were slight changes in the micromorphology of 0.1Cry and 0.5Cry (Fig. 5e and f). These results indicated the presence of dissolution–recrystallization in the charge–discharge process, which was also observed in the charge–discharge of MnO_2 in Na_2SO_4 solution (Wei et al., 2009).

The Mn AOS in tunnel-structured manganese oxides can be calculated from the normalized Mn K-edge X-ray absorption near-edge structure (XANES) spectra using the Combo method (Manceau et al., 2012). The XANES spectra of the references and fitting processes are respectively shown in Fig. S6 and Fig. S7. The fitting results of Mn K-edge XANES spectra of the 1.0Cry after charge–discharge in Cd^{2+} solutions were shown in Fig. 6a and Table S1. The Mn AOS in pristine 1.0Cry was 3.82, and was 3.87, 3.89, 3.87 and 3.85 respectively after charge–discharge in 0, 200, 600 and 1000 mg L^{-1} Cd^{2+} solutions, showing no obvious variations. The Mn K-edge k^3-weighted EXAFS spectra of pristine 1.0Cry and 1.0Cry electrode after charge–discharge in Cd^{2+} solutions further indicated that no other manganese oxides were formed after electrochemical adsorption (Fig. 6b).

3.3. *Effect of pH on electrochemical adsorption of Cd^{2+} by cryptomelane*

Fig. 7a shows the electrochemical adsorption capacities of 1.0Cry for Cd^{2+} in 1000 mg L^{-1} Cd^{2+} solutions with various initial pHs. The electrochemical adsorption capacity of 1.0Cry was 6.1 mg g^{-1} at initial pH 2.0, and increased with increasing initial pH. At initial pH 6.0, the electrochemical adsorption capacity reached 207.7 mg g^{-1}. Fig. 7b shows the corresponding XRD patterns of the 1.0Cry electrode after electrochemical adsorption at different initial pHs. No transformation of cryptomelane was observed, while the diffraction intensity of cryptomelane decreased with decreasing initial pH.

Fig. S8 shows the contents of Mn^{2+} released from 1.0Cry after charge–discharge for 50 cycles in 1000 mg L^{-1} Cd^{2+} solutions with different initial pHs. The released Mn^{2+} content showed little

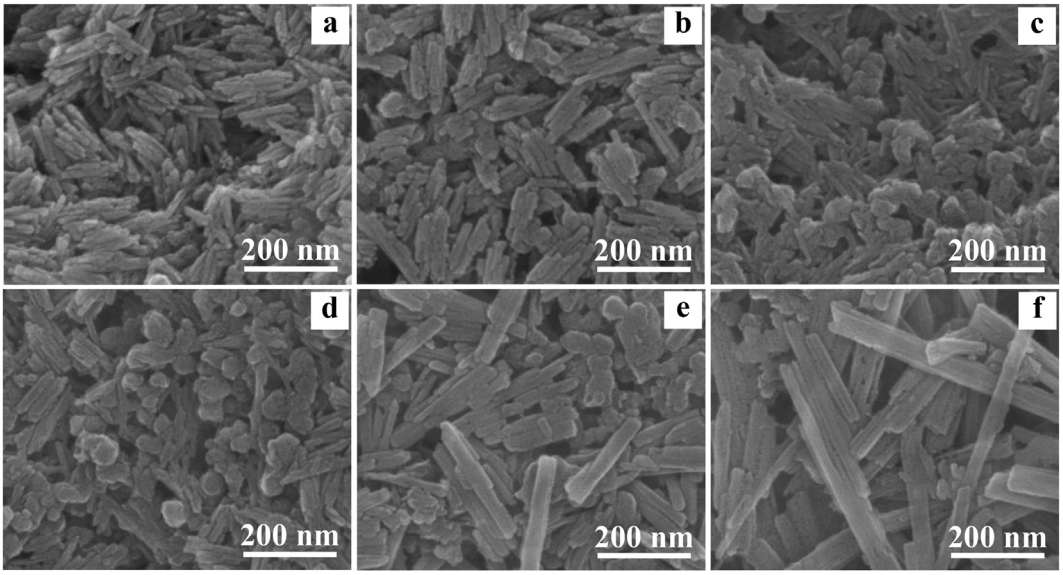

Fig. 5. FESEM images of 1.0Cry after charge–discharge for 50 cycles in 0 mg L^{-1} (a), 200 mg L^{-1} (b), 600 mg L^{-1} (c) and 1000 mg L^{-1} (d) Cd^{2+} solutions, and 0.1Cry (e) and 0.5Cry (f) after charge–discharge for 50 cycles in 1000 mg L^{-1} Cd^{2+} solution.

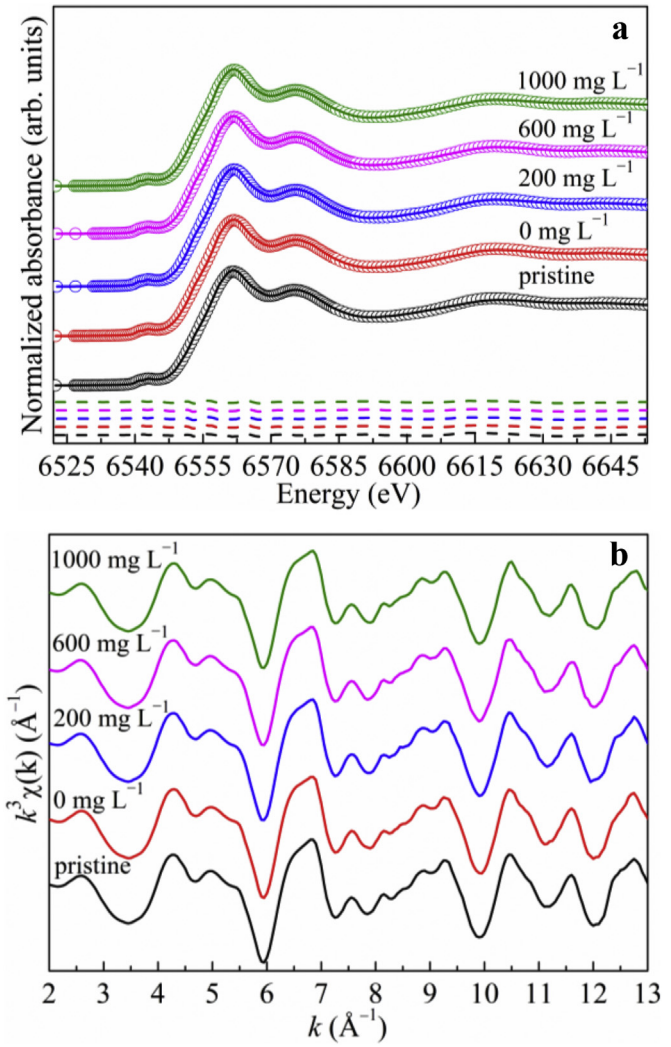

Fig. 6. Normalized Mn K-edge XANES spectra (the open circles are experimental curves; the lines are the best-fit linear combination, and difference plots are indicated at the bottom) (a) and Mn K-edge k^3-weighted EXAFS (b) of pristine 1.0Cry and 1.0Cry after charge–discharge for 50 cycles in Cd^{2+} solutions with different concentrations.

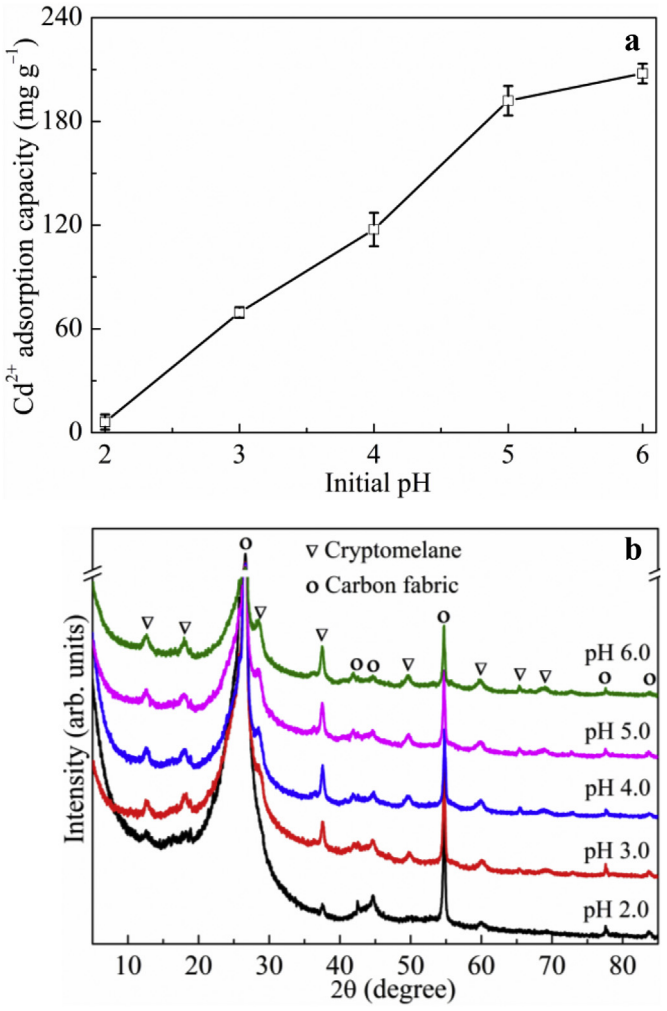

Fig. 7. Cd^{2+} adsorption capacities (a) and the corresponding XRD patterns (b) of 1.0Cry electrode after charge–discharge for 50 cycles in 1000 mg L^{-1} Cd^{2+} solution with different initial pHs.

variation between initial pH 4.0–6.0, and increased with decreasing initial pH from 4.0 to 2.0. When the initial pH was controlled at 2.0 and 3.0, the released Mn^{2+} content reached 442.7 and 262.0 mg g^{-1}, respectively.

3.4. Electrochemical adsorption of Cd^{2+} by pyrolusite and todorokite

Cyclic voltammetry test and electrochemical adsorption of pyrolusite and todorokite were performed to study the influence of the tunnel size of manganese oxides on Cd^{2+} adsorption performance. Fig. 8a shows the cyclic voltammetry plots of pyrolusite and todorokite in Cd^{2+} solutions. The integrated area of cyclic voltammetry of todorokite was larger than that of pyrolusite, indicating a higher redox activity of todorokite. Fig. 8b shows the electrochemical adsorption capacities of pyrolusite and todorokite for Cd^{2+}. With increasing Cd^{2+} concentration, the change trend in the adsorption capacity of pyrolusite and todorokite was similar to that of cryptomelane. The highest adsorption capacity of pyrolusite and todorokite was 13.5 and 44.8 mg g^{-1}, respectively, which were both lower than that of cryptomelane (192.5 mg g^{-1}). These results clearly demonstrated that the electrochemical adsorption capacities of tunnel-structured manganese oxides follow the order of cryptomelane > todorokite > pyrolusite.

Fig. S9a shows the contents of Mn^{2+} released from pyrolusite and todorokite during Cd^{2+} adsorption. With increasing Cd^{2+} concentration, the released Mn^{2+} content first increased and then reached a plateau. The highest content of Mn^{2+} released from pyrolusite and todorokite was 11.3 and 24.7 mg g^{-1}, respectively. The content of Mg^{2+} released from todorokite was about 2.0 mg g^{-1}, and changed little with increasing Cd^{2+} concentration (Fig. S9b). The XRD patterns of pyrolusite and todorokite electrodes after electrochemical adsorption indicated that no other manganese oxides were formed (Fig. S10). Dissolution–recrystallization could also be observed in FESEM images of pyrolusite and todorokite after electrochemical adsorption, and the degree of dissolution–recrystallization of cryptomelane was higher than that of pyrolusite and todorokite (Fig. S11).

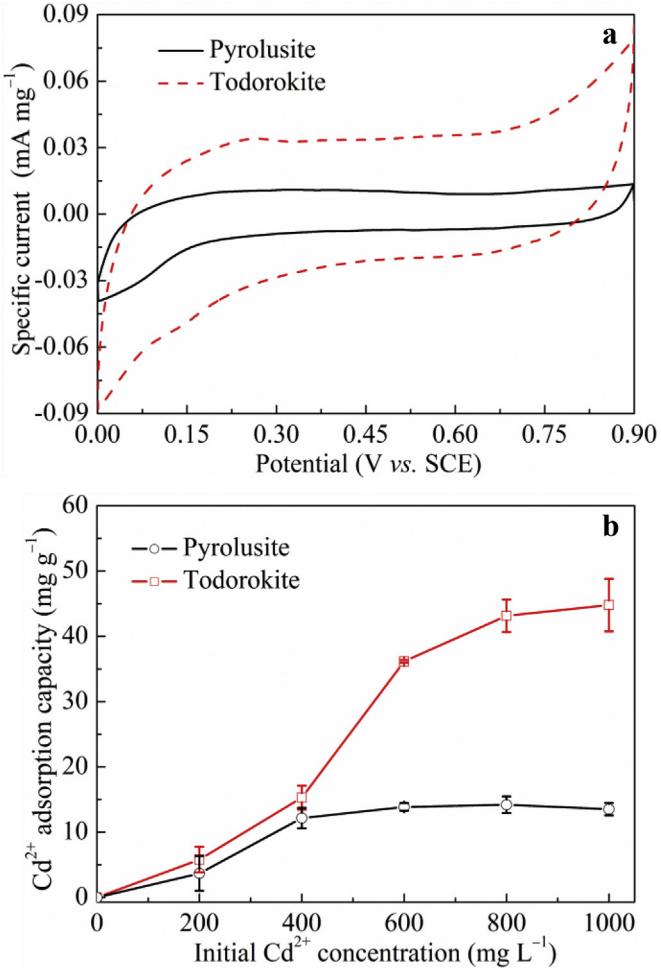

Fig. 8. Cyclic voltammetry plots for the first cycle at a scan rate of 0.5 mV s^{-1} of todorokite and pyrolusite in 1000 mg L^{-1} Cd^{2+} solution (a) and Cd^{2+} adsorption capacity of todorokite and pyrolusite after charge–discharge for 50 cycles in Cd^{2+} solutions with different concentrations (b).

4. Discussion

4.1. Electrochemical adsorption mechanism of Cd^{2+} by cryptomelane

The electrochemical adsorption capacity of Cd^{2+} was higher than the adsorption isotherm capacity (Fig. 3). The adsorption–desorption of cations occur during the redox reactions of manganese oxides: $MnO_2 + xC^+ + yH^+ + (x + y)e^- \leftrightarrow MnOOC_xH_y$, in which C^+ represents the cations in the solution such as Na^+ and K^+ (Liu et al., 2016; Simon and Gogotsi, 2008). Therefore, lithium manganese oxide ($Li_xMn_2O_4$) and sodium manganese oxide ($Na_{0.44}MnO_2$ and $Na_2Mn_5O_{10}$) have the potential to be applied in the electrochemical removal of salt ions (Lee et al., 2014; Liu et al., 2016; Zhang et al., 2018). Our previous studies have indicated that the adsorption capacity of layer-structured birnessite for heavy metal ions including Zn^{2+}, Cd^{2+} and Cu^{2+} could be improved by multi-cycle galvanostatic charge–discharge (Liu et al., 2017a; Peng et al., 2016; Yang et al., 2018). The present work indicated that the Cd^{2+} adsorption capacity of cryptomelane could also be improved by electrochemical redox reactions.

During the charge–discharge of cryptomelane in Cd^{2+} solution, the electrochemical redox reactions were incompletely reversible, as indicated by asymmetrical cyclic voltammetry plots and the higher Mn^{2+} release in the electrochemical adsorption than in the isothermal adsorption (Fig. 2 and Fig. S3). The transformation products and inner-sphere complexes formed between heavy metal ions and birnessite can lead to incomplete reversibility of the redox reactions (Liu et al., 2017a; Peng et al., 2016). In addition, dissolution–recrystallization was also observed in the electrochemical adsorption of cryptomelane for Cd^{2+} (Fig. 5). The redox reactions of manganese oxides mainly occur on the electrode surface (Ghodbane et al., 2009; Simon and Gogotsi, 2008). Dissolution–recrystallization provides a better contact between electrode materials and ions in the solution, facilitating the adsorption of cations on manganese oxides (Liu et al., 2017b). Hence, the incompletely reversible redox reactions and dissolution–recrystallization may together facilitate the enhancement of Cd^{2+} adsorption capacity.

The final pH of the solution was respectively 4.63, 4.31 and 4.08 after the electrochemical adsorption of 0.1Cry, 0.5Cry and 1.0Cry in 1000 mg L^{-1} Cd^{2+} solution, indicating the release of H^+ during the electrochemical adsorption. The tunnel of cryptomelane consists of corner-sharing and edge-sharing MnO_6 octahedral units, and the negative charges of MnO_6 octahedra are compensated by K^+ or H^+ in the tunnel (Suib, 2008; Yin et al., 2015). Cryptomelane can be used as a heavy metal ion adsorbent due to its unique structure (Suib, 2008; Yin et al., 2015). During isothermal adsorption, besides adsorption on the surface, Cd^{2+} can also be inserted into the tunnel of cryptomelane by exchanging with H^+ (Randall et al., 1998). Therefore, the exchange of H^+ by Cd^{2+} during the charge–discharge contributes to the electrochemical adsorption.

The exchange of K^+ also contributes to the electrochemical adsorption of Cd^{2+}. Only a very small proportion (2.4 mg g^{-1}) of K^+ was released from the total K^+ in 1.0Cry (48.5 mg g^{-1}) during the isothermal adsorption, indicating that it is H^+ rather than K^+ that is mainly exchanged by Cd^{2+} during isothermal adsorption. Cations can coordinate with O_2^- in the tunnel walls of cryptomelane (Randall et al., 1998). K^+ has an appropriately large radius, and can reside in the centre of the tunnel and minimize the electrostatic repulsion among O_2^- in the tunnel walls (Randall et al., 1998). Hence, H^+ is more easily exchanged by Cd^{2+} than K^+ in the tunnel (Randall et al., 1998). After the electrochemical adsorption in 1000 mg L^{-1} Cd^{2+} solution, the K^+ content in 1.0Cry decreased to 21.3 mg g^{-1}. Therefore, compared with in isothermal adsorption, the higher release of K^+ from cryptomelane also contributes to the enhancement of Cd^{2+} adsorption in electrochemical adsorption.

In the regeneration, the Cd^{2+} adsorption capacity decreased with increasing cycle number of electrochemical adsorption–desorption (Fig. 4b). The coordination of Cd^{2+} with O_2^- in the tunnel walls of cryptomelane led to the incompletely reversible redox reactions and the incomplete desorption of Cd^{2+} in the electrochemical desorption, which hindered the further electrochemical adsorption. In addition, the release of Mn^{2+} may also lead to decreases in the active manganese content and the corresponding Cd^{2+} adsorption capacity (Fig. S12).

After charge–discharge, the Mn AOS showed little change (Fig. 6a and Table S1). In our previous work, the Mn AOS of birnessite decreased after electrochemical adsorption of heavy metal ions (Liu et al., 2017a; Peng et al., 2016; Yang et al., 2018). Tunnel-structured cryptomelane has a more stable crystal structure and less surface-adsorbed Mn^{2+} compared with layer-structured birnessite. In addition, the Mn AOS values of pure cryptomelane obtained through different methods commonly varied from 3.70 to 3.90 (Feng et al., 2007; Liu et al., 2008; Polverejan et al., 2004). Therefore, no obvious change was observed in the Mn AOS after electrochemical adsorption of cryptomelane.

4.2. Influencing factors of electrochemical adsorption capacity for Cd^{2+}

The cryptomelane obtained in the reaction systems with different H_2SO_4 concentrations showed different Cd^{2+} adsorption capacities, indicating that the electrochemical adsorption capacity of cryptomelane may be affected by the chemical composition, particle size and specific surface area. At present, the effect of supporting ion K^+ in the tunnel on the electrochemical performance of cryptomelane remains unclear. The K^+ in the tunnel hinders the insertion of ions with smaller radiuses (Poyraz et al., 2017); however, K^+-cryptomelane has a more stable structure than H^+-cryptomelane, which facilitates the retention of electrochemical capacitance (Yuan et al., 2016).

The electrochemical adsorption of 1.0Cry after K^+ ion exchange in 1000 mg L^{-1} Cd^{2+} solution was performed to investigate the effect of supporting ion K^+ in the tunnel on the adsorption capacity of cryptomelane. The final pH was 4.53, and the Cd^{2+} adsorption capacity (169.4 mg g^{-1}) was lower than that of pristine 1.0Cry (192.0 mg g^{-1}). These results indicated that a high content of K^+ in the tunnel would lead to a lower Cd^{2+} adsorption capacity. However, in this work, the Cd^{2+} adsorption capacity increased with decreasing K/Mn molar ratio, which may be ascribed to the smaller particle size and higher specific surface area of 1.0Cry than those of 0.1Cry and 0.5Cry (Jiang et al., 2013). During the charge–discharge of manganese oxides, smaller particle size and higher specific surface area contribute to the electrochemical adsorption by providing more active adsorption sites (Huang et al., 2014; Jiang et al., 2013).

The Cd^{2+} adsorption capacity increased with increasing initial pH (Fig. 7a). The point of zero charge of cryptomelane is about 2.0, and the negative charge on cryptomelane surface increases with increasing pH from 2.0 to 6.0 (Feng et al., 2007). Therefore, more Cd^{2+} could be absorbed on cryptomelane. In addition, Mn^{2+} was released from cryptomelane. At initial pH 2.0 and 3.0, 82.7% and 48.9% of the Mn in the pristine 1.0Cry was released into the solution (Fig. S8), which also led to the decrease in Cd^{2+} adsorption capacity at low pHs.

The electrochemical adsorption performance of manganese oxides is also affected by their crystal structures (Figs. 3 and 8). Generally, the larger size of tunnel facilitates the insertion–extraction of cations (Ghodbane et al., 2009). The narrow tunnel (2.3 Å × 2.3 Å) of pyrolusite prevents the insertion of hydrated Cd^{2+} with a radius of 4.26 Å (Volkov et al., 1997), leading to the lowest electrochemical adsorption capacity of pyrolusite. In the case of Mg-todorokite, there are strong hydrogen bonds between the oxygen atoms in the tunnel walls and the hydrogen atoms in the magnesium hydration shell (Fig. S13) (Ghodbane et al., 2009; Post et al., 2003). The presence of hydrogen bonds can hinder the extraction of Mg^{2+} and the insertion of other cations in the solution (Ghodbane et al., 2009). In this work, only a very small proportion (2.0 mg g^{-1}) of Mg^{2+} was released from the total Mg^{2+} (450 mg g^{-1}) in todorokite during the electrochemical adsorption, further indicating that only a small number of Mg^{2+} ions were exchanged by Cd^{2+} (Fig. S9b). Hence, the electrochemical adsorption capacities of tunnel-structured manganese oxides for Cd^{2+} follow the order of cryptomelane > todorokite > pyrolusite.

Based on the principle of charge balance, 87.8, 39.1 and 22.6 mg g^{-1} of the electrochemical adsorption capacity of 1.0Cry for Cd^{2+} could be attributed to Mn^{2+} release, K^+ exchange and H^+ exchange, respectively. These results indicate that besides Mn^{2+} release, ion exchange also contributes much to the electrochemical adsorption of tunnel-structured manganese oxides for Cd^{2+}. The remaining adsorption capacity (42.5 mg g^{-1}) is likely owing to the adsorption of Cd^{2+} on the external surface of 1.0Cry (Randall et al., 1998). The specific adsorption sites and coordination environment of Cd^{2+} will be further investigated in our future study.

In our previous work, the Cd^{2+} adsorption capacity of layer-structured birnessite (900.7 mg g^{-1}) was remarkably higher than that of tunnel-structured manganese oxides (Peng et al., 2016). The interlayer spacing of birnessite is 7.2 Å, which facilitates the insertion and adsorption above/below the Mn(IV) vacancy sites of Cd^{2+} (Peng et al., 2016). In addition, the high electrochemical redox activity of birnessite led to obvious decreases in Mn AOS and crystallinity and a higher degree of dissolution–recrystallization during electrochemical adsorption. As for cryptomelane, no obvious change was observed in the structure of 1.0Cry after 400 cycles of charge–discharge in 1000 mg L^{-1} Cd^{2+} solution (Fig. S14). These results indicate that tunnel-structured manganese oxides have more stable structures than layer-structured manganese oxides, which hinder the incompletely reversible redox reactions and dissolution–recrystallization during electrochemical adsorption. Hence, layer-structured manganese oxides have higher electrochemical adsorption capacities for heavy metal ions than tunnel-structured manganese oxides.

5. Conclusions

In this study, tunnel-structured manganese oxides including pyrolusite, cryptomelane and todorokite were synthesized, and their Cd^{2+} adsorption capacities were improved by electrochemically controlled redox reactions. The enhancement of Cd^{2+} adsorption capacity could be ascribed to the dissolution–recrystallization and ion exchange during the incompletely reversible redox reactions. The Cd^{2+} adsorption capacity of cryptomelane increases with increasing pH. The K^+ present in the tunnel of H^+-cryptomelane prevents the electrochemical adsorption of Cd^{2+}. Higher specific surface area and smaller particle size contribute to Cd^{2+} adsorption capacity. The narrow tunnel of pyrolusite prevents the insertion of hydrated Cd^{2+}, leading to the lowest electrochemical adsorption of pyrolusite. The hydrogen bonds between the oxygen atoms in the tunnel walls and the hydrogen atoms in the magnesium hydration shell hinder the extraction of Mg^{2+} and the insertion of Cd^{2+}. The electrochemical adsorption capacity of tunnel-structured manganese oxides for Cd^{2+} follows the order of cryptomelane (192.0 mg g^{-1}) > todorokite (44.8 mg g^{-1}) > pyrolusite (13.5 mg g^{-1}). Overall, the present work elucidates the electrochemical adsorption mechanism of Cd^{2+} by tunnel-structured manganese oxides.

Acknowledgements

Funding for this work was provided by the National Key Research and Development Program of China (Grant Nos. 2017YFD0801000 and 2018YFD0800304), the National Natural Science Foundation of China (Grant Nos. 41571228, 41425006 and 41877025), the Fundamental Research Funds for the Central Universities (Program Nos. 2662018JC055 and 2662015JQ002). Authors owe great thanks to Dr. Lihong Qin and Dr. Jianbo Cao at the Public Laboratory of Electron Microscope in Huazhong Agricultural University for the technical assistance with SEM and TEM characterization.

Appendix A. Supplementary data

Supplementary data to this article can be found online at https://doi.org/10.1016/j.envpol.2018.10.062.

References

Chen, B.W., Wang, Y.F., Chang, Z., Wang, X.W., Li, M.X., Liu, X., Zhang, L.X., Wu, Y.P., 2016. Enhanced capacitive desalination of MnO_2 by forming composite with multi-walled carbon nanotubes. RSC Adv. 6, 6730–6736.

Dharmarathna, S., King'ondu, C.K., Pedrick, W., Pahalagedara, L., Suib, S.L., 2012. Direct sonochemical synthesis of manganese octahedral molecular sieve (OMS-2) nanomaterials using cosolvent systems, their characterization, and catalytic applications. Chem. Mater. 24, 705–712.

Feng, X.H., Tan, W.F., Liu, F., Wang, J.B., Ruan, H.D., 2004. Synthesis of todorokite at atmospheric pressure. Chem. Mater. 16, 4330–4336.

Feng, X.H., Zhai, L.M., Tan, W.F., Liu, F., He, J.Z., 2007. Adsorption and redox reactions of heavy metals on synthesized Mn oxide minerals. Environ. Pollut. 147, 366–373.

Gaikwad, M.S., Balomajumder, C., 2017. Simultaneous electrosorptive removal of chromium(VI) and fluoride ions by capacitive deionization (CDI): multicomponent isotherm modeling and kinetic study. Separ. Purif. Technol. 186, 272–281.

Ghodbane, O., Pascal, J.-L., Favier, F., 2009. Microstructural effects on charge-storage properties in MnO_2-based electrochemical supercapacitors. ACS Appl. Mater. Interfaces 1, 1130–1139.

Guo, X.J., Yang, Z., Dong, H.Y., Guan, X.H., Ren, Q.D., Lv, X.F., Jin, X., 2016. Simple combination of oxidants with zero-valent-iron (ZVI) achieved very rapid and highly efficient removal of heavy metals from water. Water Res. 88, 671–680.

Hu, C.Z., Liu, F.Y., Lan, H.C., Liu, H.J., Qu, J.H., 2015. Preparation of a manganese dioxide/carbon fiber electrode for electrosorptive removal of copper ions from water. J. Colloid Interface Sci. 446, 359–365.

Huang, M., Zhang, Y.X., Li, F., Zhang, L.L., Ruoff, R.S., Wen, Z.Y., Liu, Q., 2014. Self-assembly of mesoporous nanotubes assembled from interwoven ultrathin birnessite-type MnO_2 nanosheets for asymmetric supercapacitors. Sci. Rep. 4, 3878.

Ihsanullah, Abbas, A., Al-Amer, A.M., Laoui, T., Al-Marri, M.J., Nasser, M.S., Khraisheh, M., Atieh, M.A., 2016. Heavy metal removal from aqueous solution by advanced carbon nanotubes: critical review of adsorption applications. Separ. Purif. Technol. 157, 141–161.

Jiang, H., Lee, P.S., Li, C.Z., 2013. 3D carbon based nanostructures for advanced supercapacitors. Energy Environ. Sci. 6, 41–53.

Kijima, N., Yasuda, H., Sato, T., Yoshimura, Y., 2001. Preparation and characterization of open tunnel oxide α-MnO_2 precipitated by ozone oxidation. J. Solid State Chem. 159, 94–102.

Kim, E.-J., Lee, C.-S., Chang, Y.-Y., Chang, Y.-S., 2013. Hierarchically structured manganese oxide-coated magnetic nanocomposites for the efficient removal of heavy metal ions from aqueous systems. ACS Appl. Mater. Interfaces 5, 9628–9634.

Lee, J., Kim, S., Kim, C., Yoon, J., 2014. Hybrid capacitive deionization to enhance the desalination performance of capacitive techniques. Energy Environ. Sci. 7, 3683–3689.

Liu, L.H., Luo, Y., Tan, W.F., Liu, F., Suib, S.L., Zhang, Y.S., Qiu, G.H., 2017a. Zinc removal from aqueous solution using a deionization pseudocapacitor with a high-performance nanostructured birnessite electrode. Environ. Sci.: Nano 4, 811–823.

Liu, L.H., Qiu, G.H., Suib, S.L., Liu, F., Zheng, L.R., Tan, W.F., Qin, L.H., 2017b. Enhancement of Zn^{2+} and Ni^{2+} removal performance using a deionization pseudocapacitor with nanostructured birnessite and its carbon nanotube composite electrodes. Chem. Eng. J. 328, 464–473.

Liu, Y.-H., Hsi, H.-C., Li, K.-C., Hou, C.-H., 2016. Electrodeposited manganese dioxide/activated carbon composite as a high-performance electrode material for capacitive deionization. ACS Sustain. Chem. Eng. 4, 4762–4770.

Liu, Z.X., Xing, Y., Chen, C.H., Zhao, L.L., Suib, S.L., 2008. Framework doping of indium in manganese oxide materials: synthesis, characterization, and electrocatalytic reduction of oxygen. Chem. Mater. 20, 2069–2071.

López-Bernabeu, S., Ruiz-Rosas, R., Quijada, C., Montilla, F., Morallón, E., 2016. Enhanced removal of 8-quinolinecarboxylic acid in an activated carbon cloth by electroadsorption in aqueous solution. Chemosphere 144, 982–988.

Manceau, A., Marcus, M.A., Grangeon, S., 2012. Determination of Mn valence states in mixed-valent manganates by XANES spectroscopy. Am. Mineral. 97, 816–827.

Mohan, D., Singh, K.P., 2002. Single- and multi-component adsorption of cadmium and zinc using activated carbon derived from bagasse—an agricultural waste. Water Res. 36, 2304–2318.

Peng, Q.C., Liu, L.H., Luo, Y., Zhang, Y.S., Tan, W.F., Liu, F., Suib, S.L., Qiu, G.H., 2016. Cadmium removal from aqueous solution by a deionization supercapacitor with a birnessite electrode. ACS Appl. Mater. Interfaces 8, 34405–34413.

Polverejan, M., Villegas, J.C., Suib, S.L., 2004. Higher valency ion substitution into the manganese oxide framework. J. Am. Chem. Soc. 126, 7774–7775.

Post, J.E., 1999. Manganese oxide minerals: crystal structures and economic and environmental significance. Proc. Natl. Acad. Sci. U.S.A. 96, 3447–3454.

Post, J.E., Heaney, P.J., Hanson, J., 2003. Synchrotron X-ray diffraction study of the structure and dehydration behavior of todorokite. Am. Mineral. 88, 142–150.

Poyraz, A.S., Huang, J.P., Pelliccione, C.J., Tong, X., Cheng, S.B., Wu, L.J., Zhu, Y.M., Marschilok, A.C., Takeuchi, K.J., Takeuchi, E.S., 2017. Synthesis of cryptomelane type α-MnO_2 ($K_xMn_8O_{16}$) cathode materials with tunable K^+ content: the role of tunnel cation concentration on electrochemistry. J. Mater. Chem. 5, 16914–16928.

Qiu, G.H., Huang, H., Dharmarathna, S., Benbow, E., Stafford, L., Suib, S.L., 2011. Hydrothermal synthesis of manganese oxide nanomaterials and their catalytic and electrochemical properties. Chem. Mater. 23, 3892–3901.

Randall, S.R., Sherman, D.M., Ragnarsdottir, K.V., 1998. An extended X-ray absorption fine structure spectroscopy investigation of cadmium sorption on cryptomelane (KMn_8O_{16}). Chem. Geol. 151, 95–106.

Riederer, A.M., Belova, A., George, B.J., Anastas, P.T., 2013. Urinary cadmium in the 1999–2008 U.S. National health and nutrition examination survey (NHANES). Environ. Sci. Technol. 47, 1137–1147.

Simon, P., Gogotsi, Y., 2008. Materials for electrochemical capacitors. Nat. Mater. 7, 845–854.

Suib, S.L., 2008. Porous manganese oxide octahedral molecular sieves and octahedral layered materials. Acc. Chem. Res. 41, 479–487.

Volkov, A.G., Paula, S., Deamer, D.W., 1997. Two mechanisms of permeation of small neutral molecules and hydrated ions across phospholipid bilayers. Bioelectrochem. Bioenerg. 42, 153–160.

Wan, S.L., He, F., Wu, J.Y., Wan, W.B., Gu, Y.W., Gao, B., 2016. Rapid and highly selective removal of lead from water using graphene oxide-hydrated manganese oxide nanocomposites. J. Hazard Mater. 314, 32–40.

Wang, F., Lu, X.W., Li, X.-Y., 2016. Selective removals of heavy metals (Pb^{2+}, Cu^{2+}, and Cd^{2+}) from wastewater by gelation with alginate for effective metal recovery. J. Hazard Mater. 308, 75–83.

Wang, X., Li, Y.D., 2002. Selected-control hydrothermal synthesis of α- and β-MnO_2 single crystal nanowires. J. Am. Chem. Soc. 124, 2880–2881.

Wang, Z.M., Lee, S.-W., Catalano, J.G., Lezama-Pacheco, J.S., Bargar, J.R., Tebo, B.M., Giammar, D.E., 2013. Adsorption of uranium(VI) to manganese oxides: X-ray absorption spectroscopy and surface complexation modeling. Environ. Sci. Technol. 47, 850–858.

Wei, W.F., Cui, X.W., Chen, W.X., Ivey, D.G., 2009. Electrochemical cyclability mechanism for MnO_2 electrodes utilized as electrochemical supercapacitors. J. Power Sources 186, 543–550.

Yang, X., Liu, L.H., Tan, W.F., Qiu, G.H., Liu, F., 2018. High-performance Cu^{2+} adsorption of birnessite using electrochemically controlled redox reactions. J. Hazard Mater. 354, 107–115.

Ye, S.J., Zeng, G.M., Wu, H.P., Zhang, C., Dai, J., Liang, J., Yu, J.F., Ren, X.Y., Yi, H., Cheng, M., Zhang, C., 2017. Biological technologies for the remediation of co-contaminated soil. Crit. Rev. Biotechnol. 37, 1062–1076.

Yin, H., Dai, X.X., Zhu, M.Q., Li, F.H., Feng, X.H., Liu, F., 2015. Fe-doped cryptomelane synthesized by refluxing at atmosphere: structure, properties and photocatalytic degradation of phenol. J. Hazard Mater. 296, 221–229.

Yuan, Y.F., Zhan, C., He, K., Chen, H.R., Yao, W.T., Sharifi-Asl, S., Song, B., Yang, Z.Z., Nie, A., Luo, X.Y., Wang, H., Wood, S.M., Amine, K., Islam, M.S., Lu, J., Shahbazian-Yassar, R., 2016. The influence of large cations on the electrochemical properties of tunnel-structured metal oxides. Nat. Commun. 7, 13374.

Zhang, C.Y., He, D., Ma, J., Tang, W.W., Waite, T.D., 2018. Faradaic reactions in capacitive deionization (CDI) - problems and possibilities: a review. Water Res. 128, 314–330.

Zhang, Q., Cheng, X.H., Feng, X.H., Qiu, G.H., Tan, W.F., Liu, F., 2011a. Large-scale size-controlled synthesis of cryptomelane-type manganese oxide OMS-2 in lateral and longitudinal directions. J. Mater. Chem. 21, 5223–5225.

Zhang, Q., Xiao, Z.D., Feng, X.H., Tan, W.F., Qiu, G.H., Liu, F., 2011b. α-MnO_2 nanowires transformed from precursor δ-MnO_2 by refluxing under ambient pressure: the key role of pH and growth mechanism. Mater. Chem. Phys. 125, 678–685.

Zhao, W., Liu, F., Feng, X.H., Tan, W.F., Qiu, G.H., Chen, X.H., 2012. Fourier transform infrared spectroscopy study of acid birnessites before and after Pb^{2+} adsorption. Clay Miner. 47, 191–204.